ARTICLE

Check for updates

Grassland carbon-water cycling is minimally impacted by a photovoltaic array

Steven A. Kannenberg [1✉], Matthew A. Sturchio [1], Martin D. Venturas[2] & Alan K. Knapp[1]

Agrivoltaic systems, whereby photovoltaic arrays are co-located with crop or forage production, can alleviate the tension between expanding solar development and loss of agricultural land. However, the ecological ramifications of these arrays are poorly known. We used field measurements and a plant hydraulic model to quantify carbon-water cycling in a semi-arid C_3 perennial grassland growing beneath a single-axis tracking solar array in Colorado, USA. Although the agrivoltaic array reduced light availability by 38%, net photosynthesis and aboveground net primary productivity were reduced by only 6–7% while evapotranspiration decreased by 1.3%. The minimal changes in carbon-water cycling occurred largely because plant photosynthetic traits underneath the panels changed to take advantage of the dynamic shading environment. Our results indicate that agrivoltaic systems can serve as a scalable way to expand solar energy production while maintaining ecosystem function in managed grasslands, especially in climates where water is more limiting than light.

[1] Department of Biology and Graduate Degree Program in Ecology, Colorado State University, Fort Collins, CO, USA. [2] Departamento de Sistemas y Recursos Naturales, Universidad Politécnica de Madrid, Madrid, Spain. ✉email: steve.kannenberg@colostate.edu

In order to meet the goal of limiting global climate change, solar energy production will need to be rapidly deployed at a large scale in the coming decades[1,2]. However, solar infrastructure has extensive land requirements[3,4], and its expansion has created tension between solar development and existing land use. Agrivoltaic (AV) arrays, where solar facilities are co-located with agricultural production, have great potential to minimize this land-use tension[5]. Indeed, much of the land most suited for solar energy production tends to already be occupied by agricultural systems[6]. Agrivoltaic arrays bring notable co-benefits, including the potential for creating a more favorable microclimate for crops[7], providing shade to grazing animals[8], improving forage quality[9], and increasing farmer income and income stability[10]. While the installation of traditional solar arrays (where the land may be graded prior to construction) tends to increase soil compaction, reduce soil carbon and nutrient content, and reduce water retention[11], care can be taken during the installation phase to minimize the impacts on soil and vegetation. Such solar arrays may be better able to maintain crucial ecosystem services such as carbon storage, water retention, and habitat quality[12].

Agrivoltaic arrays are especially promising in water-limited ecosystems due to their capacity to moderate thermal environments and reduce plant water-use and soil evaporation[7]. In particular, semi-arid and arid grasslands are a favorable location for AV arrays given their short-statured vegetation and relatively flat topography. There are almost 16 million ha of grasslands managed for hay production and non-alfalfa forage in the US[13], and it has been estimated that *ca.* 4 million ha of high-density photovoltaic systems are needed to achieve the decarbonization goals of the US by 2050[14]. Thus, managed grasslands have the potential to house AV systems at a meaningful scale while concurrently increasing land-use efficiency.

However, concerns exist about the long-term impacts of AV systems including the degree to which reductions in light availability will limit plant photosynthesis, and thus forage production[9]. There are cases, though, where reductions in light intensity may be beneficial due to associated decreases in water loss and photoinhibition[7,15]. Water retention in grassland AV systems could also translate into enhanced ecosystem resistance to weather extremes such as droughts or heat waves. Overall, many uncertainties remain regarding the highly dynamic microclimate within AV systems, the physiological responses of plants to microclimate variability, and how AV arrays impact carbon and water cycling at decadal time scales[16,17]. Widespread adoption of AV in managed grasslands will depend, in part, on the degree to which ecosystem function within the array can be maintained despite reductions in light availability.

We used a well-established plant hydraulic and soil hydrology model[18,19] to simulate grassland physiology and hourly carbon-water fluxes for an AV system over a 23-year time period. The model was run at Jack's Solar Garden, a 1.5 ha, 1.2 MW single-axis tracking (i.e., panels track the sun diurnally) AV system established in 2019 near Denver, Colorado, USA. A common C_3 pasture grass (smooth brome, *Bromus inermis*) grows underneath and between the solar panels. The model was parameterized with easily measurable plant traits and driven by a combination of measured and reanalysis-derived weather data. Conceptually, we partitioned the AV system into 4 locations[20] (Fig. 1). Areas underneath the eastern (E_{edge}) and western (W_{edge}) edges of the solar panels receive additional precipitation from panel runoff, and experience full sunlight in the morning and afternoon, respectively. Locations between the panel rows (the "Between" area) experience a microclimate similar to a non-AV grassland (with the exception of minor morning and afternoon shade), while locations directly under the solar panels (the "Under" area) are mostly shaded and receive reduced direct precipitation inputs.

We compared these within-array locations to a control plot 10 m away that had similar vegetation composition and management history yet was not influenced by the solar panels.

Results and discussion

AV array impacts on ecosystem function. Annual carbon uptake (A) and evapotranspiration (ET) varied over time in response to broad trends in temperature, vapor pressure deficit, and precipitation (Fig. 2, Fig. S1). The AV array altered A and ET relative to the control plot, and these effects differed spatially. ET was elevated relative to the control plot in the E_{edge} and reduced directly underneath the panels. A in the E_{edge} and in between the panels generally matched that in the control plot but was suppressed at the W_{edge} and underneath the panels. Aboveground net primary productivity (ANPP) in 2022 somewhat reflected the trends in A, with the exception of higher ANPP in the W_{edge} than expected based on net carbon uptake (Fig. 1c). As a result, we did not find a significant linear relationship between A and ANPP across all locations. This is unsurprising given that aboveground plant growth is commonly decoupled from photosynthesis[21,22] due to direct sink limitations on growth, allocation to non-structural carbon, or belowground biomass growth. These within-AV differences reflected the balance between water and light availability. For example, the early morning sunlight received in the E_{edge} likely stimulated photosynthesis more than the afternoon sunlight received by plants at the W_{edge}, since atmospheric aridity and temperature are higher in the afternoon[20,23]. Additionally, the W_{edge} received less total sunlight due to the common presence of afternoon cloud cover (Fig. 1a). We also found that the between-panel location, though slightly shaded at the tail ends of the day, had rates of carbon uptake and water loss similar to that of the control plot. It is also notable that A for the plants directly underneath the panels was only reduced by 24.3% on average, despite an almost 70% reduction in total photosynthetic photon flux density.

We then quantified the total impact of the AV array on grassland function by scaling the responses observed in each plot by their relative area. We found that the impacts of the solar array on carbon-water cycling and plant growth were minimal compared to its effects on grassland microclimate. Across all years, the array induced an average reduction in ET of $1.3 \pm 0.9\%$ (standard deviation) and a decrease in net photosynthesis of $7.7 \pm 3\%$. Consistent with this estimate, ANPP was 6.1% lower in the AV array compared to the control plot in 2022. These small decreases in carbon-water cycling arose despite 38% reductions in total light availability (photosynthetic photon flux density summed across the entire growing season) within the AV array. The amount that ET was reduced each year varied little and was unrelated to broad climatic factors (Fig. 3). Reductions in A, though, were mediated by annual climate—for example the effect of the AV array on photosynthesis was minimized in cooler, wetter years (Fig. 3). While we lack the data to identify the mechanisms behind this result at our site, it is well-known that the response of photosynthesis to aridity and temperature is non-linear, whereby photosynthesis is strongly downregulated only when nearing critical physiological thresholds[18,24]. Given that our study site is generally hot and dry during the summer, it is likely that cooler and wetter years allow for the control plot to operate far from such thresholds, and thus more similarly to the within-AV vegetation.

While increased water savings are emerging as a common phenomenon in AV systems[7,25,26], such minor impacts on photosynthesis and productivity were striking. We found that this intriguing result can be explained by the frequent light saturation of photosynthesis in *Bromus inermis*. By measuring
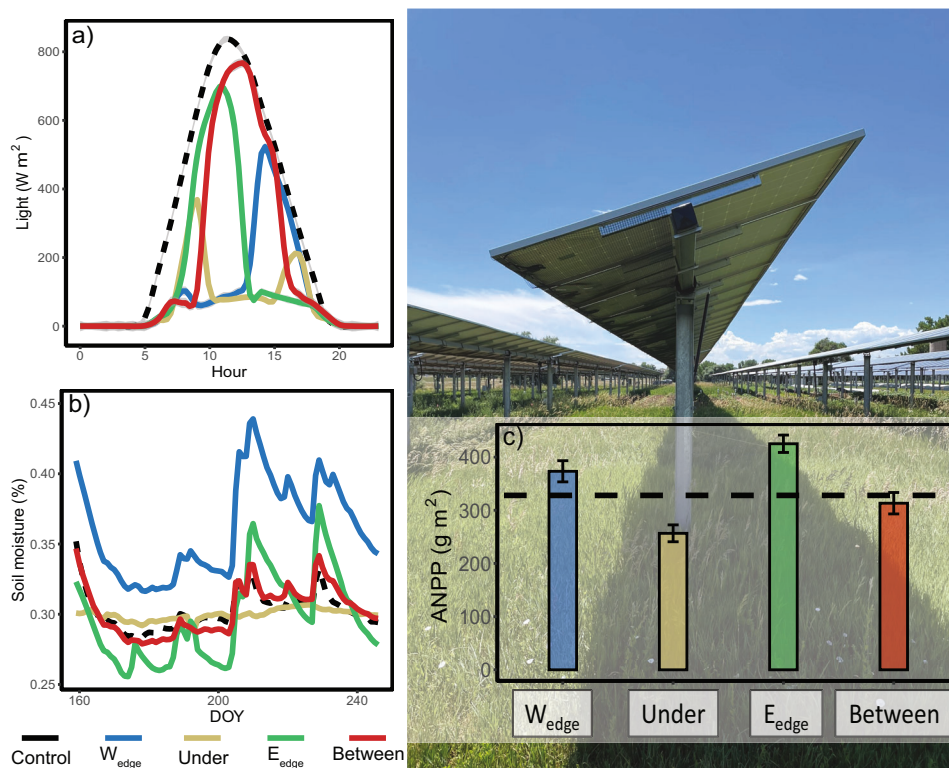
Fig. 1 Depiction of the heterogenous grassland ecosystem underneath a single-axis tracking AV array. Smoothed diurnal cycles of incoming shortwave radiation (**a**), daily soil moisture averages (**b**), and aboveground net primary productivity (ANPP) measured in September (**c**) represent data collected in 2022. The dashed line in panel **c** represents ANPP in the control plot, and its thickness corresponds to the standard error of ANPP in that plot. Error bars in panel **c** represent standard error.

light response curves in all our plots (Fig. S2), we found that photosynthesis tended to saturate at around 600 μmol photons m^{-2} s^{-1} (photosynthetic photon flux density). This light saturation point was actually closer to the light levels experienced in full shade (100–300 μmol photons m^{-2} s^{-1}) than in full sunlight (~2000 μmol photons m^{-2} s^{-1}). Even in full shade, photosynthetic rates were between 20–50% of their maximum. Thus, the partial shading of grasses was unlikely to strongly impact photosynthetic rates in most locations (except those under the panels) due to the relatively low light requirements of this perennial grass[27].

We also found large differences in photosynthetic parameters in the grasses within the AV array as compared to the non-AV control plot. Vcmax/Jmax at 25 °C, the light saturation point, and the quantum yield of photosystem II were 45%, 99%, 50%, and 48% higher (respectively) within the AV array (Figs S2–S3, Supplementary Data 1). These parameters did not differ across locations within the array, a notable finding given how similarly the between-panel plot was to the control plot in all other regards. However, this result was replicated within the AV array at our site in 2021[20] and is thus a potentially generalizable phenomenon. These photosynthetic attributes of *Bromus inermis*, along with differences in ANPP and leaf area (Fig. 1, Supplementary Data 1) likely underlie the minimal impacts of the AV array on carbon-water cycling by allowing the within-array grasses to maximize their photosynthetic rates when microclimatic conditions were favorable. Indeed, running our model with a single mean value of these photosynthetic parameters results in whole-array photosynthesis decreasing by 24.9% (on average), as compared to the 7.7% reduction when these traits were location-specific. The magnitude and directionality of this trait plasticity is somewhat

surprising, as decades of ecological research has found that plants usually decrease these parameters, not increase them, when exposed to shade[28–31]. However, much of this research has been conducted in deeply shaded forest canopies, and the elevated photosynthetic parameters inside the AV array could be due to the more favorable microclimate and/or photoinhibition in the control plot[15]. More research on photosynthesis in AV array vegetation is needed to more fully understand these trait shifts.

The impact of AV arrays on grassland function will likely differ across climates and species. While reductions in productivity are commonly observed in more mesic temperate ecosystems[9,20], drier regions may actually experience increases in plant growth under AV arrays[32,33] due to more acute water limitation in those environments. Moreover, negative effects of AV arrays on photosynthesis are likely to be more notable in C_4 species due to their higher light saturation point[34], and also in non-tracking solar arrays that have large zones of constant shade. A benefit of our modeling approach is its feasibility to address these uncertainties in other C_3 species. As long as microclimatic conditions, general weather patterns, and the traits of its constituent species are known, these questions could be tackled across a wide range of environments and species.

Our results highlight the promise of AV systems in managed semi-arid C_3 grasslands. Given that carbon-water cycling was only decreased in the under-panel plot, spacing panel rows further apart to accommodate harvesting machinery may further minimize the impacts on carbon-water cycling. Indeed, by simulating an AV system with a between-panel spacing of 6 m (an approximate average width of commonly used harvesters) we estimate reductions in scaled whole-AV ET of 4.5% and a negligible decrease in carbon uptake of 0.6%.

Can AV arrays can buffer against weather extremes? Due to reductions in mean daily leaf temperature and increases in water availability, we hypothesized that AV arrays have the potential to mitigate drought impacts in this semi-arid grassland. To test this hypothesis, we simulated the ramifications of 20% and 40% reductions in precipitation from 2000–2022, in addition to a 'hot drought' whereby reductions in precipitation were accompanied by a 5 °C increase in air temperature during the month of July (Fig. S4–S5). The simulated droughts heavily impacted carbon-water cycling, while the co-occurring heatwave had minimal impacts (Fig. 4). A 20% reduction in precipitation reduced A by $9.2 \pm 1.0\%$ (standard deviation) and ET by $14.3 \pm 1.2\%$ (standard deviation), while a 40% reduction in rain approximately doubled these decreases. The 'hot drought' further reduced A by an additional 3–5% and ET by an additional 1%. The slope of the relationship between A/ET and various climate drivers (precipitation, air temperature, and vapor pressure deficit) was not significantly different across any of these scenarios relative to the historical baseline period. The coefficient of variation in A or ET over time also did not vary notably across drought scenarios. This indicates that the AV array did not buffer the grassland from drought and heat stress, nor did it change the sensitivity of carbon-water cycling to climatic drivers.

While it is reasonable to expect that the more favorable microclimate of the AV array would confer enhanced drought resistance, this finding is perhaps expected given the ecology of semi-arid grasslands. First, grassland ecosystems are generally water limited[35], and thus reductions in thermal stress (even during droughts) may not be consequential for grass physiology. Second, we found that the negative effects of the AV array on photosynthesis were minimized in cooler, wetter years (Fig. 2b, d), and thus we

might not expect enhanced ecosystem function during simulated drought events. We also found that the effect of the solar panels relative to the controls was similar to the historical period across all drought scenarios (Fig. 4). Thus, it seems that at our site, water availability sets a top-down control on grassland function and the AV array further imparts consistent (and minor) decreases in carbon-water cycling. Indeed, this finding is in line with a large body of research indicating that grassland ecosystem function scales roughly linearly with moisture inputs[36–38]. Finally, semi-arid grasslands are adapted to seasonal water stress, and thus we may only see notable changes in how the solar array impacts ecosystem function during longer-term chronic water stress, the legacy of which lingers from one year to the next. We also note that our model does not simulate alterations in leaf area over time, which is a likely response of grasslands to weather extremes[39,40]. Drought-induced changes in photosynthetic leaf area are an unaccounted-for mechanism that could buffer the impacts of drought in this grassland.

We only simulated the impacts of drought on grassland AV function, yet other global change drivers will also ultimately shape the effects of solar panels on carbon-water cycling. In particular, rising atmospheric CO_2 concentrations might further minimize the impacts of the solar array on carbon-water cycling, due to concomitant reductions in water-use, increases in photosynthesis, or both[41,42]. This mechanism may be especially important in ecosystems that are warming past the thermal optimum of photosynthesis[43], where the shading provided by the solar panels may prove to be a net benefit. The impacts of global change on grassland ecosystems are complex and depend on interactions between CO_2, water, and nutrient availability[44–46], and understanding how these dynamics play out in AV systems will require additional experimental evidence.
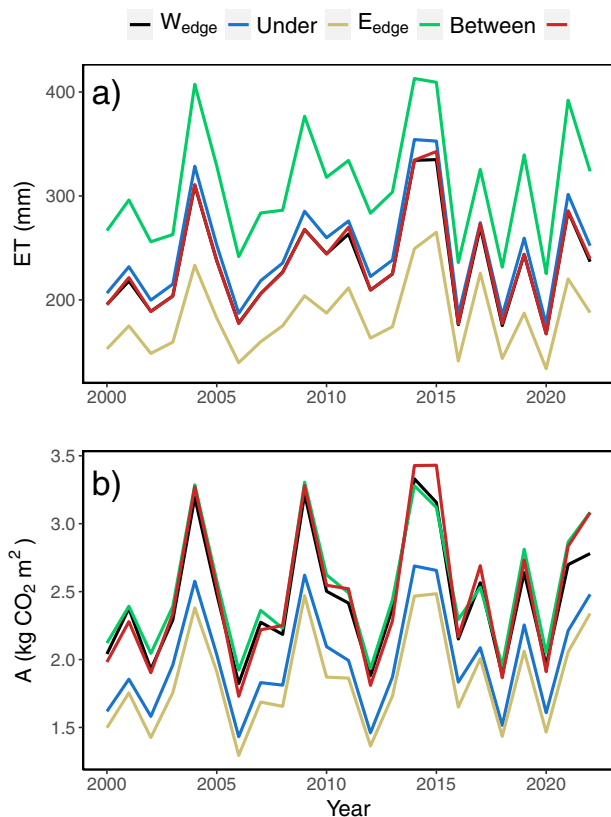
The promise of grassland AV arrays. In conclusion, we found minimal impacts of an AV array on C_3 grassland evapotranspiration, photosynthesis, and productivity, despite large reductions in light availability. These differences were underlain by sizeable spatial variability within the AV array—the E_{edge} in particular strongly benefitted from the direct morning sunlight provided by the single-axis tracking solar array. The single-axis tracking design was a key factor driving these results, as it allowed for: (a) some direct sunlight to reach the areas underneath the panels, and (b) moisture inputs to be distributed across both panels edges instead of just one (as would be the case for a fixed-angle design). The minimal impacts of the AV array likely arose due to the low degree of light limitation to photosynthesis in this semi-arid grassland, along with an alteration of photosynthetic biochemistry to take advantage of the heterogenous microclimate. However, our modeling exercise did not indicate that the increased water retention within the AV array altered grassland resistance to drought. Overall, our findings challenge the general assumption that the impacts of AV systems on light availability notably reduce photosynthesis and productivity. These findings are likely to be generalizable to other semi-arid and arid C_3 grasslands where water is more limiting than light.

Grasslands require much less management relative to other crops associated with AV systems, and their short-statured vegetation and relatively flat topography makes them ideal as candidates for solar farms. Moreover, AV systems in grasslands can be highly configurable to accommodate various harvesting equipment (by altering panel row spacing) or grazing animals (through modifying panel height). Thus, AV arrays in managed grasslands and pastures seem to be a promising path forward towards expanding solar energy production while maintaining a healthy, functioning ecosystem. While more research is needed to
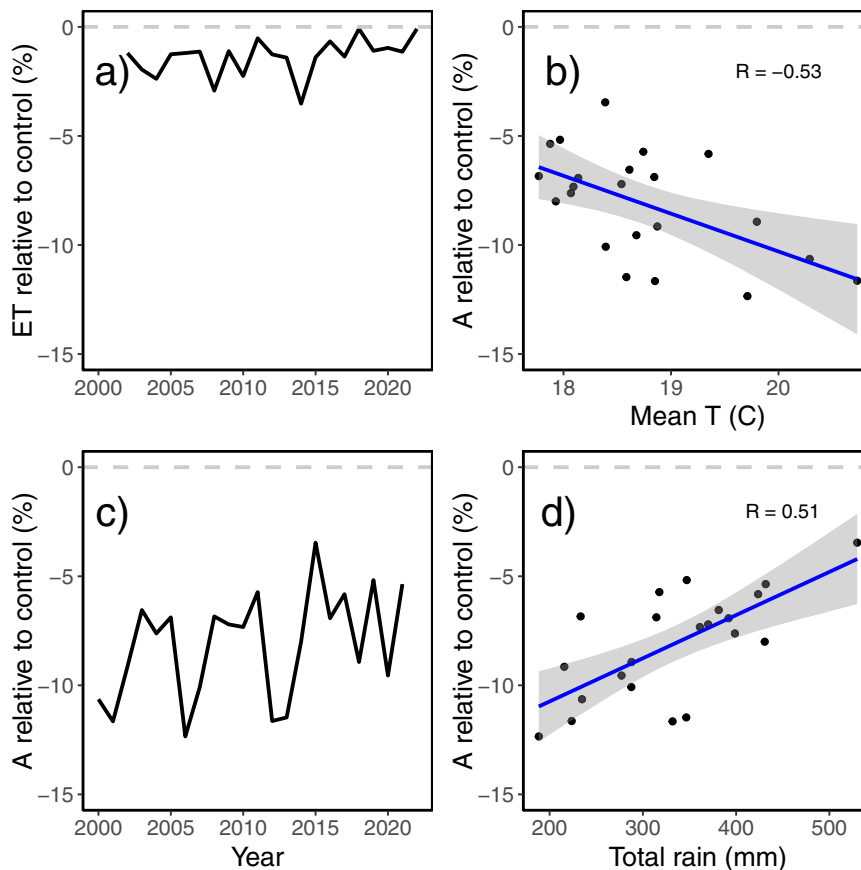

Fig. 2 Spatial differences in grassland carbon-water cycling. Time series of ET (**a**) and A (**b**) in all 5 plots from 2000–2022. Individual values represent growing season sums of carbon and water fluxes.

Fig. 3 Impacts of the AV array on spatially scaled carbon-water cycling, and the drivers of temporal variability. Whole-AV array ET (**a**) and A (**c**) relative to the control plot, where the responses observed in each plot were scaled by their area. Panels **b** and **d** show how mean air temperature (T) and precipitation mediate the difference between AV array and control photosynthesis. Blue lines indicate the linear model fit and the shaded areas are the 95% confidence intervals of that model.

quantify when, where, and how AV arrays impact ecosystem function, widespread adoption of grassland AV additionally hinges upon incentives for landowners and utility companies to expand solar energy production in a manner that prioritizes ecological health and agricultural productivity[47,48]. If properly implemented, such dual-use solar systems have great potential for enhancing financial and agricultural benefits for the farmer, as well as ecological benefits for the ecosystem.

Methods

Site. Our study site was Jack's Solar Garden in Longmont, Colorado, USA (40.12191, −105.12936). Established in 2019, Jack's Solar Garden is a 1.2 MW solar energy production facility equipped with single-axis tracking solar modules (i.e., the modules tilt east to west to follow the sun throughout the day). The solar array was installed at a flat panel height of 1.8 m, and care was taken to minimize impact on the soils and vegetation (e.g., the land was not graded). Panel rows are spaced 5.2 m apart, a design intended to prioritize energy production in single-axis tracking arrays[49,50]. Underneath the panels is a near monodominant patch of smooth brome (*Bromus inermis*), a common C$_3$ pasture grass. Some alfalfa (*Medicago sativa*) was also present, though at very low densities (<6% total ANPP), along with scattered individuals of *Dactylis glomerata* and *Tragopogon dubius*. Prior to the solar array installation, this land was a hay farm for 50 years, consisting primarily of *Bromus inermis*. The site is located at an elevation of 1526 m, and experiences a cold semi-arid climate (Köppen classification Bsk), with a mean annual temperature of 10 °C and a mean annual precipitation of 377 mm (data source: prism.oregonstate.edu).

In May 2022, we initiated a 5-plot design for sampling the ANPP and physiology of the smooth brome within, and outside, the panels. Conceptually, a single-axis tracking array can be divided into 4 regions that experience drastically different light environments and precipitation inputs[20] (Fig. 1). Plants between the panels (the "Between" area) experience some minor shade during the early morning and later afternoon and receive all the total precipitation that comes into the system. We defined the zones directly under the panel edges as "drip edges".

The drip edge on the eastern side of the panels (the "E$_{edge}$" area) receives direct sunlight in the morning and increased moisture inputs during morning rains (since the rain is redistributed from the entire panel to the E$_{edge}$). In contrast, the western drip edge (the "W$_{edge}$" area) is shaded in the morning and receives full afternoon sunlight, as well as increased moisture inputs during afternoon rains. The drip edges tend to be the wettest area of the AV array since they receive extra rain when the panel is tilted in their direction, in addition to some of the rain that occurs when the panels are tilted away (since the panel tilting in the opposite direction creates a small open space directly above the drip edge). The zone underneath the panels (the "Under" area) is heavily shaded, especially during the middle of the day, though it does get some direct light in the early morning and late afternoon. This plot does not receive any direct precipitation, so all moisture inputs percolate in from the adjacent drip edges. We also selected an undisturbed plot 10 m from the solar array to serve as a control (the "Control" plot).

To justify this plot design, Campbell Scientific CS616 soil moisture sensors were installed at a 0–15 cm depth every 20 cm within the array, and we used patterns of soil moisture following rain pulses to partition the entire AV array into these 4 zones. Via this method, the E$_{edge}$ and W$_{edge}$ were determined to extend 30 cm outwards and inwards from each panel edge (when the panels lie flat), the Under plot was the area between these edges underneath the panels, and the Between plot consisted of all the area between the panels not covered by the edges. This plot design was additionally based on spatial patterns of ANPP in 2021[20].

We measured ANPP in all 5 plots in September 2022, which was at the end of the growing season but prior to senescence. To do so, we placed 4 0.1 m^2 quadrats in each plot and clipped all vegetation by hand down to the tiller. Biomass was then dried at 60 °C for 72 h and then weighed.

Weather data. In order to drive the model described below, we generated hourly weather data from 2000–2022 from a combination of reanalysis data (from NLDAS, ldas.gsfc.nasa.gov/nldas) and measured data from our site, including: incoming photosynthetic photon flux density, precipitation, wind speed, air and soil temperature, and vapor pressure deficit. In 2022, we measured incoming photosynthetic photon flux density using Campbell Scientific CS310 sensors located within all plots of the solar array, and measured air temperature and
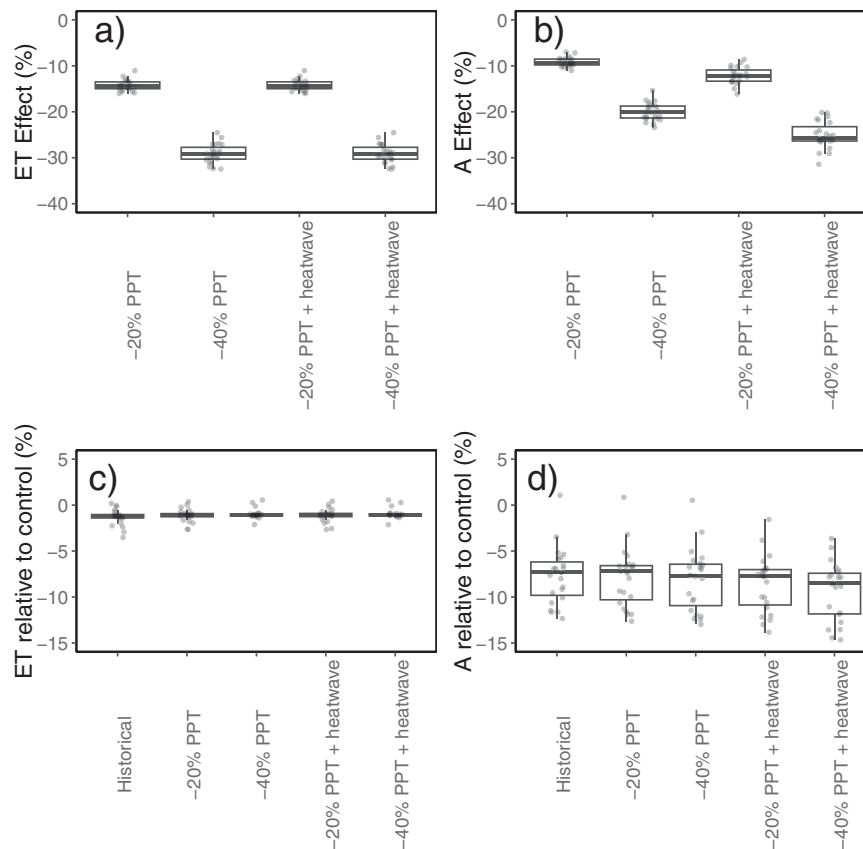
Fig. 4 Impacts of simulated droughts and hot droughts on AV array carbon-water cycling. a and **b** represent the impact of various weather extreme scenarios on annual ET and A relative to model runs from the historical period (2000–2022). **c** and **d** indicate the reductions in annual ET and A within the AV array relative to the control for all weather scenarios. The center line indicates the median, the box displays the interquartile range, and the ends of the vertical lines represent the minimum and maximum values (excluding outliers).

relative humidity at a static location underneath a solar panel using a Campbell Scientific 083E air temperature and relative humidity sensor. We then converted relative humidity to vapor pressure deficit using the R package *bigleaf*[51]. Our measurements were strongly correlated with the data from NLDAS ($r^2 = 0.91$ and $p < 0.0001$ for air temperature, $r^2 = 0.67$ and $p < 0.0001$ for vapor pressure deficit). We did not alter air temperature and vapor pressure deficit across plots due to previous evidence indicating minimal differences[52]. Our measurements were used to drive the model when present, whereas NLDAS data were used in all other circumstances. The one exception was light, since NLDAS does not incorporate the dynamic light environment caused by solar panel shading. Therefore, we applied the light data measured in all our plots in 2022 to the years 2000–2021. We acknowledge that this introduces some uncertainty in years other than 2022. However, this uncertainty is likely to be minimal, given that: (1) the relative differences in light environment across plots are extremely similar between years since the daily cycle of panel angle and seasonal cycle of sun angle will not change, and (2) the total amount of solar radiation at our site does not differ much year-to-year (coefficient of variation = 0.015).

Estimating the amount of precipitation received by each plot is challenging since we could not install a precipitation gauge directly in each plot. Even if we could, this would not be realistic since it does not account for any lateral water movement between plots. Thus, we estimated plot-specific moisture inputs based on the dynamics of soil moisture following a precipitation event. First, we identified precipitation events of >5 mm in a given day. Next, we calculated the percentage increase in post-precipitation soil moisture (1 day after) relative to pre-precipitation moisture (1 day prior) in the drip edge plots, standardized by the percentage increase in soil moisture experienced by the between-panel plot (which receives no extra precipitation from panel runoff). Thus, this percentage represents the 'extra' moisture received under the panel drip edges due to panel runoff. We then applied this scalar to our precipitation data in the drip edge plots. This method was not valid for our under-panel plot, however, as that plot showed no increase in soil moisture following precipitation. However, the under-panel plots receiving no moisture is clearly not realistic since soil moisture in our under-panel plot did not decline over the year, and was similar in magnitude to our control plot despite getting little to no direct precipitation (Fig. 1b). Soil water in this plot likely percolates in from the drip edge soils at slower time scales. Therefore, we estimated the under-panel plot precipitation scalar by varying it from 10%–90% in 2022, and

choosing the value (70%) with the lowest root mean square error between measured and modeled water potential.

Model description. We used a well-established plant hydraulics model (the "Sperry model"[18,19]) to simulate net photosynthesis (A), evapotranspiration (ET), and plant water potential (Ψ) in each of the 5 plots over the past 23 years. We ran the model from May 1 to August 31 in order to capture the growing season, while avoiding the initial growth and senescence processes that the model is unable to capture. Briefly, this model simulates plant gas exchange based on a novel optimization criterion that maximizes the difference between standardized photosynthetic gain relative to the risk of hydraulic conductivity loss. Soil water availability is determined via a single layer 'bucket' type hydrology model, where soil water potential is determined based on soil texture, evaporation, and plant water demand. The model is parameterized with plant traits (Supplementary Data 1) and driven by weather data at an hourly timestep. This model has been shown to equal other empirical models in performance[19], with the added benefit that such a trait-based model is more easily applied across species and systems and can better simulate novel conditions like weather extremes or climate change[53]. Model traits unique to our site and species are available in Supplementary Data 1, and were measured in each plot (see below) or extracted for *Bromus inermis* from the TRY database[54]. The remaining model parameters that were not specific to our study are available in Sperry et al.[18] and Venturas et al.[19].

While this model has been previously applied mostly to woody plants, the underlying physiology is highly applicable to grasses given one key modification—enabling losses of hydraulic conductivity to be instantaneously reversed when water potentials get less negative. Mathematically, this means that instead of conductivity losses being permanent, plant hydraulic conductivity returns to the value corresponding to the new water potential, determined by its hydraulic vulnerability curve. While the occurrence and mechanisms of embolism refilling in woody vegetation remains contentious[55], we believe this to be a necessary modification to properly represent grass hydraulics for three reasons. First, most conductivity loss in leaves is likely not due to embolism, but to xylem conduit deformation and/or loss of extra-xylary conductance[56–58]. Such conductivity losses are rapidly reversible upon rehydration. However, we do note that this is an emerging view and there is very little research to date on grasses. Second, in short-statured plants,

nighttime refilling of embolized xylem is possible due to positive root pressures[59], especially when soils are relatively moist as was the case during our study period (Fig. 1). Third, our measurements of water potential (described below) approached or even exceeded the P50 of *Bromus inermis* (the point of 50% conductivity loss) during most of the growing season (Figs. S6–S10), despite soil moisture levels that were fairly high. Given that P50 in woody plants is thought of as a critical threshold that defines severe water stress[60], we contend that the most plausible explanation for the fact that this grass species remains alive and photosynthesizing is that losses of conductivity can be reversed on short time scales.

Model traits. Vcmax and Jmax were extracted from A-Ci curves that were measured using a Licor 6800. Between 6–8 A-Ci curves were measured at Ci levels of 420, 300, 250, 150, 100, 50, 0, 420, 650, 800, 1200, 1500, in June and July for the within-array plots, and 3 curves were measured in control plots in July. Photosynthetically active radiation inside the chamber was set to 1800 μmol m^{-2} s^{-1}. Light response curves were also measured with a Licor 6800 in June and July at descending photosynthetically active radiation values of from 2500 to 0 μmol m^{-2} s^{-1}, and a CO_2 concentration of 420 ppm. 9–10 light response curves per plot were constructed for the within-array plots, and 5 were constructed for the control plot. For all curves, the flow rate was set to 600 μmol s^{-1} and the chamber temperature and humidity was set to match ambient conditions. Gas exchange measurements were then appropriately scaled using measurements of leaf area in the chamber. All curves were measured in the morning or early afternoon to avoid stomatal closure associated with aridity or temperature. Vcmax and Jmax were calculated using the R package *plantecophys*[61], while the light compensation point was calculated with the R package *photosynthesis*[62].

Leaf area index was measured 3 times in each plot with a METER ACCUPAR LP-80 in June, July, and August. Leaf area index values did not notably change throughout the summer so the mean value for each plot was used. Leaf area per unit tiller area was calculated on a subset of 20 grass blades sampled in June. Leaf area was measured on each ramet with a Licor 3100-C leaf area meter, and tiller area was measured with digital calipers. Tiller area per unit ground area was calculated similarly, where the number of tillers was estimated in quadrats across all plots in June, a mean tiller area was estimated with digital calipers, and tiller area per unit ground area was calculated by multiplying the number of tillers by the mean area. These two traits did not differ significantly across plots, and thus mean values were used in the model.

Finally, two of the model parameters are either impossible to measure accurately or need to be tuned to fit empirical data: (1) soil moisture at the start of the model run (as a percent of field capacity), and (2) the percentage of whole-plant hydraulic resistance contributed by the rhizosphere. To estimate these parameters, we ran the model in 2022 while varying each parameter from 10–90% in increments of 10%, and picked the resulting values that minimized root mean square error between measured and modeled plant water potential (see section below).

Model validation. We validated the model by comparing measurements of plant water potential to modeled daily values across various timepoints. To collect validation data, we measured plant water potential with a PMS 600 Scholander-type pressure chamber every two weeks from May 2022–August 2022 (June 2022–August 2022 for the control plot). On each of these days, we took 3 measurements per within-array plot across 3 different transects spaced ~5 m apart (9 measurements total in each plot) and 3 measurements in the control plot. We repeated these measurements at 5 timepoints: 9 am, 11 am, 1 pm, 3 pm, and 5 pm (Figs. S6–S10). Before measurement, grass blades were bagged for 5–10 min and recut at a standardized location to avoid artifacts due to differences in leaf gas exchange along the length of the leaf blade[63].

In general, measured and modeled plant water potential varied in magnitude little over the course of a relatively wet growing season, with the exception of a transient dry-down period near DOY 170. Modeled water potential replicated the magnitude of measured water potential fairly well, with the exception of simulating more negative pressures in some plots during the dry-down period. The root mean square error across all plots was 1.13 MPa, and varied between plots from 0.92 to 1.37 MPa. We also note that there was very high variability in measured plant water potential, even within the same plot at a given time point, and our model is unable to capture this variability. Indeed, in many cases the variability in water potential at a given time in a given plot approached or exceeded the variability in mean water potential over the growing season. This variability could arise due to differences in leaf angle, light availability, and rooting depth, though we did not measure these variables directly. However, we did find high variability in Vcmax and Jmax within individuals in a given plot, as the coefficient of variation for Vcmax varied from 0.19–0.47 between plots, and from 0.28–0.42 for Jmax. This variability in photosynthetic parameters could be another mechanism contributing to intraspecific differences in water potential.

Simulating drought impacts on grassland AV function. In order to simulate the impacts of the photovoltaic array on drought resistance, we simulated the impacts of flat reductions of 20% and 40% in each precipitation event from 2000–2022. We also simulated a 'hot drought', where precipitation was altered as above in addition

to a 5 °C increase in air temperature during the month of July; VPD was also recalculated during this month based on air temperature. We note that it is our intention here to generate a first-order approximation of how drought impacts grassland AV array carbon-water cycling, not simulate actual droughts, other climate extremes, or climate change impacts.

Data availability

References

1. Creutzig, F. et al. The underestimated potential of solar energy to mitigate climate change. *Nat. Energy* **2**, 17140 (2017).
2. IPCC. Mitigation of climate change-summary for policymakers. *IPCC Clim. Change 2022* (IPCC, 2022).
3. Hernandez, R. R. et al. Environmental impacts of utility-scale solar energy. *Renew. Sustain. Energy Rev.* **29**, 766–779 (2014).
4. Hernandez, R. R., Hoffacker, M. K. & Field, C. B. Efficient use of land to meet sustainable energy needs. *Nat. Clim. Change* **5**, 353–358 (2015).
5. Macknick, J., Beatty, B. & Hill, G. *Overview of Opportunities for Co-Location of Solar Energy Technologies and Vegetation*. NREL/TP--6A20-60240, 1115798 http://www.osti.gov/servlets/purl/1115798/ (2013).
6. Adeh, E. H., Good, S. P., Calaf, M. & Higgins, C. W. Solar PV power potential is greatest over croplands. *Sci. Rep.* **9**, 1–6 (2019).
7. Barron-Gafford, G. A. et al. Agrivoltaics provide mutual benefits across the food–energy–water nexus in drylands. *Nat. Sustain.* **2**, 848–855 (2019).
8. Maia, A. S. C., de Andrade Culhari, E., de França Carvalho Fonsêca, V., Milan, H. F. M. & Gebremedhin, K. G. Photovoltaic panels as shading resources for livestock. *J. Clean. Prod.* **258**, 120551 (2020).
9. Andrew, A. C., Higgins, C. W., Smallman, M. A., Graham, M. & Ates, S. Herbage yield, lamb growth and foraging behavior in agrivoltaic production system. *Front. Sustain. Food Syst.* **5**, 1–12 (2021).
10. Dinesh, H. & Pearce, J. M. The potential of agrivoltaic systems. *Renew. Sustain. Energy Rev.* **54**, 299–308 (2016).
11. Yavari, R., Zaliwciw, D., Cibin, R. & McPhillips, L. Minimizing environmental impacts of solar farms: a review of current science on landscape hydrology and guidance on stormwater management. *Environ. Res. Infrastruct. Sustain.* **2**, 032002 (2022).
12. Walston, L. J. et al. Opportunities for agrivoltaic systems to achieve synergistic food-energy-environmental needs and address sustainability goals. *Front. Sustain. Food Syst.* **6**, https://doi.org/10.3389/fsufs.2022.932018 (2022).
13. USDA. *Crop Production 2021 Summary*. (USDA, 2022).
14. Ardani, K. et al. *Solar Futures Study* (U.S. Department of Energy Solar Energy Technologies Office, 2021).
15. Adams, W. W., Muller, O., Cohu, C. M. & Demmig-Adams, B. May photoinhibition be a consequence, rather than a cause, of limited plant productivity? *Photosynth. Res.* **117**, 31–44 (2013).
16. Barron-Gafford, G. A. et al. The photovoltaic heat island effect: larger solar power plants increase local temperatures. *Sci. Rep.* **6**, 35070 (2016).
17. Guoqing, L. et al. Ground-mounted photovoltaic solar parks promote land surface cool islands in arid ecosystems. *Renew. Sustain. Energy Transit.* **1**, 100008 (2021).
18. Sperry, J. S. et al. Predicting stomatal responses to the environment from the optimization of photosynthetic gain and hydraulic cost. *Plant Cell Environ.* **40**, 816–830 (2017).
19. Venturas, M. D. et al. A stomatal control model based on optimization of carbon gain versus hydraulic risk predicts aspen sapling responses to drought. *New Phytol.* (2018) https://doi.org/10.1111/nph.15333.
20. Sturchio, M. et al. Grassland productivity responds unexpectedly to dynamic light and soil water environments induced by photovoltaic arrays. *Ecosphere* https://doi.org/10.1002/ecs2.4334 (2022).
21. Cabon, A. et al. Cross-biome synthesis of source versus sink limits to tree growth. *Science* **376**, 758–761 (2022).
22. Körner, C. Paradigm shift in plant growth control. *Curr. Opin. Plant Biol.* **25**, 107–114 (2015).
23. Lin, C. et al. Evaluation and mechanism exploration of the diurnal hysteresis of ecosystem fluxes. *Agric. For. Meteorol.* **278**, 107642 (2019).
24. Moore, C. E. et al. The effect of increasing temperature on crop photosynthesis: from enzymes to ecosystems. *J. Exp. Bot.* **72**, 2822–2844 (2021).

25. Adeh, E. H., Selker, J. S. & Higgins, C. W. Remarkable agrivoltaic influence on soil moisture, micrometeorology and water-use efficiency. *PLoS ONE* **13**, e0203256 (2018).

26. Ravi, S. et al. Colocation opportunities for large solar infrastructures and agriculture in drylands. *Appl. Energy* **165**, 383–392 (2016).

27. Sekiyama, T. & Nagashima, A. Solar sharing for both food and clean energy production: performance of agrivoltaic systems for corn, a typical shade-intolerant crop. *Environ. MDPI* **6**, 65 (2019).

28. Boardman, N. K. Comparative photosynthesis of sun and shade plants. *Annu. Rev. Plant Physiol.* **28**, 355–377 (1977).

29. Hernández, G. G., Winter, K. & Slot, M. Similar temperature dependence of photosynthetic parameters in sun and shade leaves of three tropical tree species. *Tree Physiol.* **40**, 637–651 (2020).

30. Kubiske, M. E., Zak, D. R., Pregitzer, K. S. & Takeuchi, Y. Photosynthetic acclimation of overstory Populus tremuloides and understory Acer saccharum to elevated atmospheric CO_2 concentration: Interactions with shade and soil nitrogen. *Tree Physiol.* **22**, 321–329 (2002).

31. Rosati, A., Esparza, G., DeJong, T. M. & Pearcy, R. W. Influence of canopy light environment and nitrogen availability on leaf photosynthetic characteristics and photosynthetic nitrogen-use efficiency of field-grown nectarine trees. *Tree Physiol.* **19**, 173–180 (1999).

32. Graham, M. et al. Partial shading by solar panels delays bloom, increases floral abundance during the late-season for pollinators in a dryland, agrivoltaic ecosystem. *Sci. Rep.* **11**, 1–13 (2021).

33. Liu, Y. et al. Solar photovoltaic panels significantly promote vegetation recovery by modifying the soil surface microhabitats in an arid sandy ecosystem. *Land Degrad. Dev.* **30**, 2177–2186 (2019).

34. Pearcy, R. & Ehleringer, J. Comparative ecophysiology of C3 and C4 plants. *Plant Cell Environ.* **7**, 1–13 (1984).

35. Churkina, G. & Running, S. W. Contrasting climatic controls on the estimated productivity of global terrestrial biomes. *Ecosystems* **1**, 206–215 (1998).

36. Knapp, A. K. et al. Rainfall variability, carbon cycling, and plant species diversity in a Mesic Grassland. *Science* **298**, 2202–2205 (2002).

37. Nippert, J. B., Knapp, A. K. & Briggs, J. M. Intra-annual rainfall variability and grassland productivity: can the past predict the future? *Plant Ecol.* **184**, 65–74 (2006).

38. Sala, O. E., Parton, W. J., Joyce, L. A. & Lauenroth, W. K. Primary production of the central grassland region of the United States. *Ecology* **69**, 40–45 (1988).

39. Han, D. et al. Hydroclimatic response of evapotranspiration partitioning to prolonged droughts in semiarid grassland. *J. Hydrol.* **563**, 766–777 (2018).

40. Zha, T. et al. Interannual variation of evapotranspiration from forest and grassland ecosystems in western canada in relation to drought. *Agric. For. Meteorol.* **150**, 1476–1484 (2010).

41. Berry, J. A., Beerling, D. J. & Franks, P. J. Stomata: key players in the earth system, past and present. *Curr. Opin. Plant Biol.* **13**, 232–239 (2010).

42. Field, C., Jackson, R. & Mooney, H. Stomatal responses to increased CO_2: implications from the plant to global scale. *Plant Cell Environ.* **18**, 1212–1225 (1995).

43. Duffy, K. A. et al. How close are we to the temperature tipping point of the terrestrial biosphere? *Sci. Adv.* **7**, eaay1052 (2021).

44. Hovenden, M. J. et al. Warming prevents the elevated CO_2-induced reduction in available soil nitrogen in a temperate, perennial grassland. *Glob. Change Biol* **14**, 1018–1024 (2008).

45. Pan, Y. et al. Contrasting responses of woody and grassland ecosystems to increased CO_2 as water supply varies. *Nat. Ecol. Evol.* **6**, 315–323 (2022).

46. Mueller, K. E. et al. Impacts of warming and elevated CO_2 on a semi-arid grassland are non-additive, shift with precipitation, and reverse over time. *Ecol. Lett.* **19**, 956–966 (2016).

47. Pascaris, A. S., Schelly, C. & Pearce, J. M. A first investigation of agriculture sector perspectives on the opportunities and barriers for agrivoltaics. *Agronomy* **10**, 1885 (2020).

48. Pearce, J. M. Agrivoltaics in Ontario Canada: promise and policy. *Sustainability* **14**, 3037 (2022).

49. Appelbaum, J. & Aronescu, A. Inter-row spacing calculation in photovoltaic fields—a new approach. *Renew. Energy* **200**, 387–394 (2022).

50. Mayer, M. J. Impact of the tilt angle, inverter sizing factor and row spacing on the photovoltaic power forecast accuracy. *Appl. Energy* **323**, 119598 (2022).

51. Knauer, J., El-Madany, T. S., Nke Zaehle, S. & Migliavacca, M. Bigleaf-An R package for the calculation of physical and physiological ecosystem properties from eddy covariance data. *PLoS ONE* **13**, e0201114 (2018).

52. Marrou, H., Guilioni, L., Dufour, L., Dupraz, C. & Wery, J. Microclimate under agrivoltaic systems: Is crop growth rate affected in the partial shade of solar panels? *Agric. For. Meteorol.* **177**, 117–132 (2013).

53. Sperry, J. S. et al. The impact of rising CO_2 and acclimation on the response of US forests to global warming. *Proc. Natl. Acad. Sci. USA.* **116**, 25734–25744 (2019).

54. Kattge, J. et al. TRY plant trait database—enhanced coverage and open access. *Glob. Change Biol.* **26**, 119–188 (2020).

55. Venturas, M. D., Sperry, J. S. & Hacke, U. G. Plant xylem hydraulics: What we understand, current research, and future challenges. *J. Integr. Plant Biol.* **59**, 356–389 (2017).

56. Brodribb, T. J. & Holbrook, N. M. Water stress deforms tracheids peripheral to the leaf vein of a tropical conifer. *Plant Physiol.* **137**, 1139–1146 (2005).

57. Scoffoni, C. et al. Outside-xylem vulnerability, not Xylem embolism, controls leaf hydraulic decline during dehydration. *Plant Physiol.* **173**, 1197–1210 (2017).

58. Zhang, Y. et al. Xylem conduit deformation across vascular plants: an evolutionary spandrel or protective valve? *New Phytol.* https://doi.org/10.1111/nph.18584 (2022).

59. Sperry, J. S., Holbrook, N. M., Zimmermann, M. H. & Tyree, M. T. Spring filling of xylem vessels in wild grapevine. *Plant Physiol.* **83**, 414–417 (1987).

60. Brodribb, T. J. & Cochard, H. Hydraulic failure defines the recovery and point of death in water-stressed conifers. *Plant Physiol.* **149**, 575–584 (2009).

61. Duursma, R. A. Plantecophys—an R package for analysing and modelling leaf gas exchange data. *PLoS ONE* **10**, e0143346 (2015).

62. Stinziano, J., Roback, C., Murphy, B., Mudson, P. & Muir, C. *Photosynthesis: Tools for Plant Ecophysiology & Modeling.* https://github.com/cdmuir/photosynthesis (2022).

63. Ocheltree, T. W., Nippert, J. B. & Prasad, P. V. V. Changes in stomatal conductance along grass blades reflect changes in leaf structure. *Plant Cell Environ.* **35**, 1040–1049 (2012).

Acknowledgements

Author contributions

S.A.K. designed the study, collected field data, ran the model, analyzed the data, and wrote the manuscript. M.A.S. designed the study, collected field data, and contributed to writing the manuscript. M.D.V. developed model code, provided guidance on running the model, and contributed to writing the manuscript. A.K.K. designed the study and contributed to writing the manuscript.

Competing interests

The authors declare no competing interests.

Additional information